
Electrochemically Addressable Trisradical Rotaxanes Organized Within a Metal–Organic Framework

Paul R. McGonigal,[†] Pravas Deria,[†] Idan Hod,[†] Peyman Z. Moghadam,^{||} Alyssa-Jennifer Avestro,[†] Noah E. Horwitz,[†] Ian C. Gibbs-Hall,[†] Anthea K. Blackburn,[†] Dongyang Chen,[†] Youssry, Y. Botros,^{†,||} Michael R. Wasielewski,[†] Randall Q. Snurr,^{||} Joseph T. Hupp,[†] Omar K. Farha,^{†,¶} J. Fraser Stoddart,^{†,*}

[†]Department of Chemistry and ^{||}Department of Chemical and Biological Engineering, Northwestern University, Evanston, IL 60208, USA. [¶]National Center for Nano Technology Research, King Abdulaziz City for Science and Technology, P.O. Box 6086, Riyadh 11442, Kingdom of Saudi Arabia, ^{||}Intel Labs, Building RNB-6-61, 2200 Mission College Boulevard, Santa Clara, CA 95054, USA, [¶]Department of Chemistry, Faculty of Science, King Abdulaziz University, Jeddah 22254, Kingdom of Saudi Arabia.

Abstract

The organization of trisradical rotaxanes within the channels of a Zr₆-based metal-organic framework (NU-1000) has been achieved post-synthetically by Solvent-Assisted Ligand Incorporation. Robust Zr^{IV}-carboxylate bonds are forged between the Zr clusters of NU-1000 and carboxylic acid groups of rotaxane precursors (semirotaxanes) as part of this building block replacement strategy. UV-Vis-NIR, EPR and ¹H NMR spectroscopies all confirm the capture of redox-active rotaxanes within the mesoscale hexagonal channels of NU-1000. Cyclic voltammetry measurements performed on electroactive thin films of the resulting material indicate that redox-active viologen subunits located on the rotaxane components can be accessed electrochemically in the solid state. In contradistinction to previous methods, this strategy for the incorporation of mechanically interlocked molecules within porous materials circumvents the need for *de novo* synthesis of a metal-organic framework, making it a particularly convenient approach for the design and creation of solid-state molecular switches and machines. The results presented here provide proof-of-concept for the application of post-synthetic transformations in the integration of dynamic molecular machines with robust porous frameworks.

Significance Statement

The research paper presents a strategy for the organization of artificial molecular switches based on mechanically interlocked molecules within a porous crystalline framework. Once arranged within the pores of the framework, the electronic state of the switches can be altered by the application of an electrochemical potential. This strategy is particularly useful when it comes to integrating dynamic, stimulus-responsive, mechanically interlocked molecules with the robustness and periodicity of porous solids. The findings of the research establish proof-of-concept for the application of post-synthetic transformations of porous crystalline frameworks in the creation of solid-state molecular switches and machines.

The predictability and reliability with which metal–organic frameworks (MOFs) are assembled (1–11) has accelerated the rate at which porous materials can be developed for applications as diverse as gas storage and separation (7), sensing (8), catalysis (9), and light harvesting (10–11). Metal oxide joints and organic struts are arranged regularly within MOFs, giving rise to hybrid materials with permanent porosities. It has been proposed (12–13) that integrating the rigidity and periodicity of MOFs with the addressability and workings of molecular switches and machines, such as bistable mechanically interlocked molecules (MIMs) (14–16), stands a good chance of giving rise to a new class of functional materials that are simultaneously both robust and dynamic. Most switchable MIMs that have been developed operate in solution where they are stochastically oriented and the net movement of a population of switches averages to zero. By integrating such rudimentary molecular switches within highly ordered MOFs, however, they can be organized periodically and precisely in 3D space, allowing their otherwise incoherent motions to be rectified. While steady progress has been made (17–26) toward this goal in recent years, it still remains a considerable challenge to design such systems that can be addressed by stimuli in the solid state. Electrochemical potential and light would be particularly appealing stimuli on account of their ease of interfacing with current technologies. The avenues of investigation that have been explored up to this point have entailed the *de novo* assembly of MOFs from MIMs that double as organic struts—ones that are bulkier and considerably more complex than those routinely employed in the preparation of MOFs. Consequently, laborious and demanding optimization of solvothermal crystallization conditions has often been necessary in order to grow MOFs from the MIM struts.

During these past 15 years we have devoted a considerable amount of time and effort in research into manipulating the self-organization of relatively small numbers of bistable MIMs as a means of storing and processing information in defect-tolerant architectures in order to realize both memory and logic functions in molecular electronic devices (MEDs). We made the decision at the outset of what turned out to be a fruitful collaboration (Fig. 1) with James (Jim) Heath, starting in 2000 with the publication of an article (27) in *Science* describing the solid-state electronically reconfigurable switch based on a bistable [2]catenane, to work with collections of molecules, rather than with single molecules, for two reasons – one being that we were looking for a relatively simple way of tiling bistable MIMs into device settings where multiple junctions (points) are individually and separately addressable, and the other being that isolated single molecules cannot be relied upon to reside passively in a particular state: we decided it made much more sense to put our trust in collections of molecules where even if some – obeying the Boltzmann distribution – were out of sync with the rest, then the majority of the molecules would cover for them. The devices, which were chosen right at the beginning, were based on crossbar architectures (27, 28) for the simple reason that thousands at least, if not hundreds, of molecules could, in principle, be addressed uniquely and separately inside molecular switch tunnel junctions (MSTJs) corresponding to the crossing points of the wires associated with these crossbar architectures. We established a highly repeatable fabrication method in which the Langmuir-Blodgett (LB) technique

is employed to self-organize the bistable catenanes and rotaxanes on these crossbars: the fact that the LB technique is commensurate with the tiling of molecules in two dimensions means that we can deliver monolayers of the bistable MIMs with relative ease and in surprisingly high efficiency to the MSTJs on the crossbars. We were also to discover, as a result of carrying out an extensive piece of physical organic chemistry (29), that, when these bistable MIMs – which can be switched electrochemically in solution – are introduced into highly viscous polymer matrices, self-assembled as monolayers on gold surfaces courtesy of thiooctic acid appendages, or organized by their hundreds or thousands between two wires (electrodes) at MSTJs, the thermodynamics which characterize their switching remains invariant, whereas their kinetics are influenced as expected – they go from being fast (half-life-times of seconds) in solution to being slow (half-life-times of hours) in crossbar MSTJs. This program of research hit its high spot in 2007 with the publication of an article (30) in *Nature* describing a 160-kilobit molecular electronic memory patterned at 100,000,000,000 bits per square centimeter with bistable [2]rotaxane molecules, which exhibit a footprint somewhere in the region of 2 nm² in an LB film, serving as the data storage elements. The assembled crossbar memory consisted of 400 Si bottom-nanowire electrodes (16 nm wide, 33 nm pitch) crossed by 400 Ti top-nanowire electrodes (16 nm wide, 33 nm pitch), sandwiching a monolayer of approximately 100 bistable [2]rotaxane molecules. There are some major limitations hampering the further development of MEDs based on bistable MIMs: one is the non-scalable LB technique for forming densely packed monolayers of the MIMs free of defects and the other is the fact that the devices tend to peter out after tens, or at the most, hundreds of cycles. A relatively recent attempt (31) to introduce a switchable, multiply bistable polyrotaxane by spin-coating it onto the bottom Si electrode met with only limited success. In retrospect, this observation is hardly all that surprising since structural failure along the polymer backbone is to be expected when it is subjected to repeated dynamics. These lessons have led us to believe (12, 32) that the means of improving device robustness may reside in MOFs which are capable of housing bistable MIMs without compromising their ability to switch, courtesy of the relative movements of their components. A more lengthy discussion of our foray into molecular electronics is presented (32) in *Chemical Society Reviews* published in 2012. In a perspective entitled “Whence Molecular Electronics” featured (33) in *Science* in 2004, it was concluded that —

“Molecular electronics will mature into a powerful technology only if its development is based on sound scientific conclusions that have been tried and tested at every step. Reaching these objectives requires a detailed understanding of the molecule / electrode interface, as well as developing methods for manufacturing reliable devices and ensuring their robustness.”

MOFs (1–11) are highly self-assembled crystalline compounds with porous structures comprised of metal-oxide joints and organic struts that extend in all directions throughout the crystal: the molecule is the crystal and the crystal is the molecule! In a perspective on “Robust Dynamics” published (12) in *Nature Chemistry* in 2010, we proposed, in conjunction (Fig. 1) with Omar Yaghi, coupling the dynamics exhibited by molecular switches and machines in bistable MIMs

with the rigid two- and three-dimensional structures associated with MOFs so as to yield materials that are intrinsically robust yet exhibit dynamics. The prospect of positioning molecular switches symmetrically within the constitutions of organic struts of MOFs, or attaching them to the metal-oxide joints of MOFs, is an attractive proposition. We argued that, if the mounting of bistable MIMs in MOFs could be achieved, then it would afford us a class of solid-state devices which could open up fresh opportunities in the field of molecular electronics.

Two architectural features can be distinguished in the majority of porous MOFs with reference to the pore apertures and the internal sorting and coverage domains. In the sorting domain, molecules are selected at the orifices of the pores, according to their sizes. In the coverage domain, molecules are adsorbed by weak van der Waals forces associated with the struts and metal-joints. In 2009, we introduced (34) a third domain – an active one – into a MOF in the form of a crown ether and demonstrated that it is capable of binding methyl viologen (MV^{2+}). The docking of MV^{2+} in MOF-1001, where the struts incorporate a bisparaphenylene[34]crown-10 (BPP34C10) established that donor-acceptor molecular recognition between BPP34C10 and MV^{2+} , which is well-known to occur in solution, can be transferred with its receptor function being preserved into a MOF. The success of this experiment, based on the cubic topology of the archetypal MOF-5, in which paraphenylene struts are joined by $Zn_4O(CO_2)_6$ cluster joints, places the concept of robust dynamics on a firm footing.

Our subsequent attempts to incorporate struts containing a degenerate [2]catenane, in which the BPP34C10 ring – or a 1,5-dioxynaphthalene-containing analogue thereof – is interlocked mechanically with the tetracationic cyclophane, cyclobis(paraquat-*p*-phenylene) (**CBPQT**⁴⁺) which contains two viologen units, met with only limited success, and that was only after the zinc nitrate employed in the synthesis of MOF-1001 was replaced by copper nitrate.

In 2010, we reported (19) the synthesis and crystal structure of MOF-1011 in which a donor-acceptor [2]catenane, obtained by using a dicarboxylic acid containing a BPP34C10 ring interlocked with a **CBPQT**⁴⁺ cyclophane, is incorporated into a solid-state, two-dimensional network replete with ordered catenanes – one per copper unit, eight per unit cell, and 81 per 100 nm² surface – throughout the crystal. An extended strut, wherein 1,5-naphthoparaphenylene[34]crown-10 (NPP36C10) was grafted into its midriff prior to being catenated with **CBPQT**⁴⁺ cyclophanes, has been employed (18) in the preparation of MOF-1030 which constitutes an example of the ordering of MIMs within a well-defined three-dimensional solid matrix. The catenated MOF-1030, however, brings the prototypically active switching machinery in the struts to a standstill! This phenomenon was not an entirely unfamiliar one. The changes in dynamic behavior that can be expected upon transitioning from working in solution, where molecules are free to tumble randomly, to crystalline materials, where they are highly ordered and densely packed, has been investigated systematically (35, 36) by Miguel Garcia-Garibay (Fig. 1) for several years. The additive effect of the many strong short-range interactions between closely-

packed molecules often arrests large-amplitude molecular motion almost entirely. Rapid dynamics are favored by large free volumes, weak intermolecular interactions, and high symmetry. Not only did the MIM components of MOF-1011 and MOF-1030 fill most of the free volume that would otherwise have been present in the MOF, they also possessed complementary donor and acceptor π -surfaces that could interact favorably with one another.

When two – one degenerate and the other nondegenerate – [2]catenanes, containing struts incorporating NPP36C10 and bearing two terphenylene arms were reacted in the presence of copper nitrate, the copper-paddlewheel-based MOF-1050 and MOF-1051 were isolated (24) as crystalline compounds. The solid-state structures of these MOFs reveal that the metal clusters serve to join the heptaphenylene struts into gridlike two-dimensional sheets that are then held together by infinite donor-acceptor stacks involving the [2]catenanes to produce interpenetrated three-dimensional architectures. Our frustration at the fact that π - π stacking interactions always seems to come into play between donor-acceptor catenanes when they are incorporated into MOFs and hence arrest the relative movements of the rings which could lead to switching behavior has found some recompense in MOF-2000, obtained when a mixture of struts containing a crown ether (BPP34C10) and a [2]catenane – with BPP34C10 and **CBPQT**⁴⁺ mechanically interlocked – are reacted with zinc nitrate in *N,N*-dimethylformamide at 65° C. The creation of MOF-2000, whose two components are incorporated always in precisely a 2:1 ratio, even when the ratio of the two struts in the reaction mixture are varied by an order of magnitude, is a profound observation. We have just recently reported (37) in the *Proceedings of the National Academy of Sciences* statistical mechanical modeling by Stephen (Steve) Whitelam which suggests that the robust 2:1 ratio has a nonequilibrium origin which results from kinetic trapping of the two different struts during the growth of the framework of MOF-2000. The timeline presented in Fig. 2 summarizes the progress that has been made in harnessing the switching the switching properties of bistable MIMs in MEDs and the subsequent attempts to house MIMs inside MOFs.

While this article was being written up for publication, Stephen Loeb (Fig. 1) has described, in an article (38) published in *Nature Chemistry*, the design and synthesis of a molecular shuttle that operates inside a Zn-based MOF that is a two-fold interpenetrated, cubic lattice in which the two frameworks are not connected covalently, i.e., they are catenated. A wide range of dynamic ¹³C NMR experiments were performed on the crystalline MOF which demonstrate that a [24]crown-8 (24C8) ring undergoes a degenerate shuttling motion between two benzimidazole recognition sites in a molecular shuttle positioned in an H-like manner between two triphenyldicarboxylic acid struts employed in the synthesis of the MOF. The rate of shuttling of the 24C8 ring in the MOF is associated with an energy barrier of 14.1 kcal mol⁻¹, which is considerably higher than the energy barrier of the 7.7 kcal mol⁻¹ observed for the strut by itself dissolved in a deuterated toluene solution. While several reasons are advanced for this difference in the free energy of activation between the solution and solid states, an intriguing, but unlikely, possibility is that “one ring cannot move without its motion requiring the next ring to move.”

Here, we outline a strategy for the organization of MIMs within the channels of a premade MOF through post-synthetic building block replacement. A semirotaxane (39), which is first formed in solution, binds (Fig. 3A) to coordination sites within the MOF through a functional end group at its non-stoppered end. It is thus immobilized within the pores of the framework while simultaneously undergoing a transformation to a kinetically trapped rotaxane in which the MOF serves as the second stopper. In addition to characterizing the resulting framework by UV-Vis-NIR, EPR and ^1H NMR spectroscopies, we have also conducted a molecular mechanics investigation in order to gain further insight into the experimentally observed number of mechanically interlocked (rotaxane) and non-interlocked (dumbbell) components within the pores. We have grown electroactive thin films of the MOF crystals and demonstrated that redox-active subunits located on the rotaxane components can be accessed electrochemically in the solid state during cyclic voltammetry.

Results and Discussion

Design Strategy. Recently we reported (40–42) the preparation of **NU-1000**, a mesoporous Zr-based MOF with trihexagonal channels. **NU-1000** is composed (Fig. 3B) of octahedral hexa-Zr joints and tetratopic 4,4',4'',4'''-(pyrene-1,3,6,8-tetrayl)tetrabenzoate linkers (**PyTBA**) with a molecular formula of $\text{Zr}_6(\mu_3\text{-O})_4(\mu_3\text{-OH})_4(-\text{OH})_4(-\text{OH}_2)_4(\text{PyTBA})_2$. The eight non-bridging $-\text{OH}$ and $-\text{OH}_2$ groups of the Zr clusters are oriented toward the center of the 30 Å-wide hexagonal channels and, hence, present the opportunity for chemical modification. We anticipated that these spatially oriented functional handles would be convenient attachment points as part of our strategy to organize MIMs inside a MOF.

We have developed (43–45) a general building block replacement protocol, namely Solvent-Assisted Ligand Incorporation (SALI), based on the displacement of Zr-bound aqua and hydroxyl ligands of **NU-1000** by exogenous carboxylic acid or phosphonic acid derivatives. The charge-compensating κ^2 -coordination of the acid derivatives to the oxophilic Zr clusters in the SALI daughter MOFs is a thermodynamically favorable and particularly robust bonding motif (41, 46). Against this background, we designed a prototypical system (Fig. 4A) based on $\mathbf{1}^{2+}$, a benzoic acid derivative that can participate in SALI while also possessing the requisite structural features for semirotaxane formation. The viologen unit (47) at the center of the half-dumbbell $\mathbf{1}^{2+}$ was chosen as a recognition site to promote complexation with **CBPQT** $^{4+}$ by virtue of radical templation (46–54). A bulky 3,5-di-*tert*-butylphenyl stopper situated at the other end of the viologen unit ensures that the semirotaxanes become mechanically interlocked once the benzoic acid group is capped by the Zr cluster. The synthesis of $\mathbf{1}\cdot 2\text{PF}_6$ was completed in three steps from commercially available materials with an overall yield of 48%. See the supporting information.

Semirotaxane Formation. Simultaneous reduction of the benzoic acid derivative and the ring to form $\mathbf{1}^{+\bullet}$ and $\mathbf{CBPQT}^{2(++)}$, respectively, is necessary in order to establish attractive noncovalent bonding interactions between the host and the guest in solution. It is only in their radical cation redox states that favorable interactions (47–56) between the electrons of the viologen centers bring the components together to form (Fig. 4B) the trisradical semirotaxane $\mathbf{1}^{+\bullet}\subset\mathbf{CBPQT}^{2(++)}$. Complexation was observed (Fig. 4C) by spectroelectrochemistry conducted in MeCN solution with 0.1 M Bu_4NPF_6 as the supporting electrolyte. An equimolar solution of $\mathbf{1}\cdot 2\text{PF}_6$ and $\mathbf{CBPQT}\cdot 4\text{PF}_6$ was prepared in a cuvette under an inert N_2 atmosphere and subjected to a potential (–330 mV) that is sufficient to induce one-electron reduction of the viologen subunits of both the ring (54) and the half-dumbbell component (Fig. S1). A change from colorless to a deep blue/green color was observed as the reduction proceeded and UV-Vis-NIR spectroscopy confirmed (Fig. 4C) the formation of the semirotaxane $\mathbf{1}^{+\bullet}\subset\mathbf{CBPQT}^{2(++)}$. The broad absorbance observed in the near-IR at 1167 nm, which we attribute to a charge transfer-type electronic transition from the SOMO (50) of the semirotaxane, has been established (48–56) as a spectroscopic signature of similar trisradical viologen inclusion complexes.

In addition to electrochemical stimulus, the one-electron reduction of the viologen subunits and subsequent semirotaxane formation can also be achieved using chemical reductants (47–56) such as Zn dust or cobaltocene (CoCp_2) in an appropriate stoichiometry. UV-Vis-NIR Spectra confirmed (Fig. S2) the expected formation of $\mathbf{1}^{+\bullet}\subset\mathbf{CBPQT}^{2(++)}$ upon chemical reduction. Solutions of $\mathbf{1}^{+\bullet}\subset\mathbf{CBPQT}^{2(++)}$ (8 mM with respect to $\mathbf{1}^{+\bullet}$) were prepared for SALI by the addition of $\text{Co}(\text{Cp}_2)$ to mixtures of $\mathbf{1}\cdot 2\text{PF}_6$ and $\mathbf{CBPQT}\cdot 4\text{PF}_6$ in anhydrous, deaerated MeCN under the inert N_2 atmosphere of a glovebox. An excess (2.5 equiv) of the ring component was used in order to bias (Fig. 3A) the equilibrium in favor of semirotaxane formation.

Solvent-Assisted Ligand Incorporation. SALI is performed (43, 44) by adding the MeCN solution of $\mathbf{1}^{+\bullet}\subset\mathbf{CBPQT}^{2(++)}$ to a microcrystalline sample of freshly activated **NU-1000** and heating the heterogeneous mixture at 60 °C under an inert N_2 atmosphere for 18 h with occasional swirling. See Materials and Methods. Under these conditions, the semirotaxane diffuses through the channels of the MOF crystals and is captured as a result of coordination to the Zr clusters through SALI. After cooling the mixture to room temperature, the supernatant of the reaction mixture is drawn off and the powder is soaked in fresh, deaerated MeCN, before decanting the solvent and repeating the procedure three more times in order to remove any residual unbound $\mathbf{1}^{+\bullet}$ or $\mathbf{CBPQT}^{2(++)}$. The framework produced is labeled **SALI-R**³⁽⁺⁺⁾, where ‘SALI’ indicates that it is part of the SALI MOF family (43, 44, 46) and ‘R³⁽⁺⁺⁾’ denotes the presence of $\mathbf{1}^{+\bullet}\subset\mathbf{CBPQT}^{2(++)}$ -derived rotaxanes within the extended structure.

A portion of **SALI-R**³⁽⁺⁺⁾ was digested in a D_2SO_4 – $(\text{CD}_3)_2\text{SO}$ mixture and analyzed by ¹H NMR spectroscopy to verify the presence of rotaxanes within the framework. The spectrum reveals

(Fig. 5A) the presence of both $\mathbf{1}^{2+}$ and \mathbf{CBPQT}^{4+} in addition to the $\mathbf{D}_4\mathbf{PyTBA}$ linker. The fact that the ring is retained inside the framework, despite its inability to coordinate to the Zr clusters, is consistent with it being captured within the channels as part of a kinetically trapped rotaxane structure. Comparison of the integrals of non-overlapping signals associated with the viologen protons of $\mathbf{1}^{2+}$ and \mathbf{CBPQT}^{4+} — $\text{H}_{\alpha-\text{d}}$ and $\text{H}_{\alpha+\beta}$, respectively—with those corresponding to the \mathbf{PyTBA} linker (H_{BA}) allows us to determine the amount of rotaxane that is retained within $\mathbf{SALI-R}^{3(++)}$. A molar ratio of approximately 4:2 \mathbf{PyTBA} to $\mathbf{1}^{2+}$ is apparent, indicating that, on average, each hexagonal section of the framework houses three dumbbells. Approximately half of these dumbbells are encircled by a ring, as evidenced by the 2:1 ratio of $\mathbf{1}^{2+}$ to \mathbf{CBPQT}^{4+} . The observation of a mixture of dumbbells and rotaxanes reflects the equilibrium nature of the complexation in solution.

More direct evidence of the presence of $\mathbf{1}^{+} \subset \mathbf{CBPQT}^{2(++)}$ -derived rotaxanes within the MOF was obtained by examining (Fig. 5B) the microcrystalline $\mathbf{SALI-R}^{3(++)}$ powder by UV-Vis-NIR reflectance spectroscopy. A comparison was made with two control frameworks, namely $\mathbf{SALI-DB}^{2+}$ and $\mathbf{SALI-DB}^{(++)}$, which were prepared by performing SALI in the absence of the \mathbf{CBPQT}^{4+} ring component with solutions of $\mathbf{1}^{2+}$ and $\mathbf{1}^{+}$, respectively. See the supporting information. A broad peak centered around 1120 nm was apparent in the case of $\mathbf{SALI-R}^{3(++)}$, but not in the spectra of the two control frameworks. The near-IR absorbance is a consequence of the trisradical rotaxanes, confirming their presence within the framework material and, hence, the viability of our strategy for post-synthetic formation of MIMs inside $\mathbf{NU-1000}$. Samples of $\mathbf{SALI-DB}^{(++)}$ and $\mathbf{SALI-R}^{3(++)}$ were also analyzed (Fig. 6A) by EPR spectroscopy, which verified the presence of unpaired electrons (57) in both of the materials, as would be anticipated. Although the presence of crystals with multiple orientations relative to the applied magnetic field prevents resolution of individual hyperfine splittings in these samples, the broad, featureless signals that are centered around $g = 2$ are typical of polycrystalline solid samples containing organic radicals. Spin exchange and dipolar interactions between radicals in close proximity may contribute to the signal broadening.

In order to assess the stability of $\mathbf{SALI-DB}^{(++)}$ and $\mathbf{SALI-R}^{3(++)}$ to oxidation, the impact of air exposure on the EPR and UV-Vis-NIR signals was investigated. Firstly, we monitored the rate of oxidation by measuring (Fig. 6B) the decay in EPR signal intensities—i.e., the second integral of the field-modulated EPR spectra—that proceeds immediately after the samples of $\mathbf{SALI-DB}^{(++)}$ and $\mathbf{SALI-R}^{3(++)}$ are opened to the air, along with the broadening of the signals. Both materials appear to exhibit a biexponential decay in signal intensity with a short lifetime on the order of minutes and a longer one on the order of hours. Similar oxidation behavior was observed by recording solid-state UV-Vis-NIR reflectance spectra of the $\mathbf{SALI-DB}^{+}$ (Fig. 6C) and $\mathbf{SALI-R}^{3(++)}$ (Fig. 6D) microcrystalline powders after the cuvettes were opened to the air. The signals in the visible and near-infrared regions corresponding to radical species diminished rapidly at first over a period of approximately an hour and then at a slower rate thereafter, finally reaching completion after a period of 2–4 days. For comparison, a solution of $\mathbf{1}^{+} \subset \mathbf{CBPQT}^{2(++)}$ in MeCN was exposed

to air and its UV-Vis-NIR spectra recorded (see Fig. S3) at 5-minute intervals. The absorbance at 1167 nm associated with the trisradical complex decayed completely within 10 minutes and no trace of any absorbances indicative of other radical species remained after 70 minutes. Although these solution-phase experimental conditions were necessarily different from those used to monitor the decay of radical species in the solid state (different cuvettes were used, for example), a qualitative comparison of the timescales for oxidation suggests that the radical species are slightly more resistant to oxidation when organized inside the metal–organic framework – compare the timescale of a few minutes for decay of the trisradical complex in the solution sample versus approximately an hour for the same process in the microcrystalline framework. A contributing factor to this apparent stabilization could be a difference in the rate of O₂ diffusion in the crystal compared to solution. With the ultimate goal of applying MOFs such as **SALI-R**³⁽⁺⁺⁾ in the context of MEDs, further enhancement of its stability to atmospheric oxygen would be desirable, either by modifying the structure of the molecular switch or treating the MOF with a coating that isolates it from its surrounding atmosphere.

In Silico Modeling. The proportion of **1**⁺⁺ that is incorporated in **SALI-R**³⁽⁺⁺⁾, either as a non-interlocked dumbbell or as part of a rotaxane, amounts to only one quarter of the theoretical maximum. Up to four exogenous carboxylates can be accommodated (43, 45) around a single Zr cluster of **NU-1000**, whereas an average of only one rotaxane or dumbbell component per cluster was observed (Fig. 5A) experimentally in the case of **SALI-R**³⁽⁺⁺⁾. In order to gain further insight, we employed molecular mechanics to model (Fig. 7 and Fig. S12) a short section of a hexagonal pore containing different distributions of dumbbells and rotaxanes. See Materials and Methods. Comparison of the energies of the structural analogues relative to combined energies of the isolated pore, dumbbells, and rotaxanes, gives an indication as to whether or not a particular arrangement of rings and dumbbells is favorable. A pore containing six dumbbells and three rings distributed across 12 Zr clusters (two hexagons) was evaluated (Fig. 7A) as its composition reflects the stoichiometry of **SALI-R**³⁽⁺⁺⁾. The model reveals that, although the components come into close contact with one another at the center of the channel, the arrangement of three dumbbells or rotaxanes per hexagon allows sufficient space for the contents of the channel to pack without large distortions. This is reflected in its corresponding energy (E) of approximately $-65 \text{ kcal mol}^{-1}$. By contrast, modeling predicts (Fig. 7B) a large destabilization ($\sim 779 \text{ kcal mol}^{-1}$) if six dumbbell or rotaxane components are confined within a single hexagon – a situation that would occur if the proportion of carboxylate derivatives is doubled to two per cluster. In the model, congestion at the center of the channel is compensated for by relatively large distortions in the dumbbell components, causing them to bend back toward the periphery of the channel. Although the effects of counterions, solvent, and conformational isomerism of the pyrenyl linkers are not accounted for in the model, qualitatively, the *in silico* study is consistent, with the experimentally observed preference of fewer than two carboxylate derivatives per cluster. When designing more advanced

MIMs to take part in a SALI strategy in the future, it may be useful to first assess their likely distribution within the framework by computational modeling.

Thin-Film Electrochemical Studies. Electrophoretic deposition can be employed (58, 59) to deposit microcrystallites of **NU-1000** on conductive fluorine-doped tin oxide (FTO) transparent electrodes. We have shown previously (58, 59) that the majority of **PyTBA** linkers can be accessed electrochemically in the resulting thin films. SALI was performed on a **NU-1000**–FTO electrode in order to obtain thin films of **SALI-R**³⁽⁺⁺⁾ (Fig. 8A) that could be studied electrochemically. A cyclic voltammogram was acquired (Fig. 8B) using a standard three-electrode configuration featuring a Ag/AgCl reference electrode and a Pt-mesh counter electrode submerged in a 0.1 M TBAPF₆ solution in MeCN as supporting electrolyte. By sweeping to negative potential, a semi-reversible reduction wave is observed at –250 mV. As no part of the **NU-1000** framework itself (including the **PyTBA** linker) is susceptible to reduction at this potential, we attribute this peak to the one electron reduction of the viologen components that are confined within its channels. In order to elucidate the proportion of viologen-containing components that can be addressed electrochemically in **SALI-R**³⁽⁺⁺⁾ we measured (Fig. 8C) the passage of current over time after a step in potential from 100 mV to –700 mV. The experiment revealed that 43% of the viologen units of **SALI-R**³⁽⁺⁺⁾ are electroactive.

Conclusions

We have established that a straightforward chemical modification strategy allows MIMs to be arranged inside a premade MOF prior to being addressed electrochemically. In the present case, rotaxanes that originate from short, rigid trisradical semirotaxanes are trapped inside the channels of **NU-1000** as part of the SALI building block replacement method. The Zr-cluster-centered SALI technique is highly modular (43–46), which bodes well for the application of this method in the context of other types of mechanically interlocked molecules and supramolecular systems. The mild and versatile conditions should make this approach compatible with a range of molecular recognition motifs, while it would also be possible to incorporate fully formed rotaxanes or catenanes in place of the semirotaxanes exemplified here. One could also envision that flexible MIMs with dimensions larger than the diameter of the hexagonal channels of **NU-1000** may even be compatible if they are capable of extending along the channels. This modular method will be a valuable tool in the development of functional materials that are simultaneously both robust and dynamic. We have demonstrated that a significant proportion of the redox-active MIMs can be addressed electrochemically after being immobilized in the MOF. The ability to control redox-active switches within a robust porous framework would be particularly appealing in the context of molecular electronic devices (30, 32, 60, 61). The results establish proof-of-concept for the application of post-synthetic transformations of porous crystalline frameworks in the creation of solid-state molecular switches (62, 63) and molecular machines.

Materials and Methods

Procedure for the preparation of SALI-R^{3(••)}. A solution of **1**•2PF₆ (29.6 mg, 40 μmol) and **CBPQT**•4PF₆ (110 mg, 100 μmol) in anhydrous, deaerated MeCN (5.0 mL) was prepared under an inert N₂ atmosphere in a glovebox. Another solution of CoCp₂ (46.0 mg, 240 μmol) in anhydrous, deaerated MeCN (2.5 mL) was added dropwise with swirling, resulting in a color change from colorless to intense dark green/blue. This solution was then added to a 60 mg portion of activated **NU-1000** (0.027 mmol) under inert atmosphere in a 20 mL microwave vial (Biotage). The sealed vial was heated at 60 °C for 18 h with occasional swirling. After cooling to room temperature, the supernatant of the reaction mixture was decanted and the MOF sample was soaked in fresh deaerated MeCN, before decanting the solvent and repeating the procedure three more times. Finally, the MOF sample was dried under vacuum and a portion was analyzed ¹H NMR spectroscopy after digesting in D₂SO₄ and diluting with (CD₃)₂SO (1:9 final ratio), which indicated (Fig. 5A) the incorporation of approximately 0.5 equiv of **1**⁺⊂**CBPQT**^{2(••)} and 0.5 equiv of free **1**⁺ per Zr cluster.

Molecular Mechanics Modeling. In order to gain further insight into how the presence of rotaxanes in the **NU-1000** framework affects the energetics, we modeled different rotaxane-functionalized structures based on classical molecular mechanics energy minimization. The initial coordinates for **NU-1000** were taken from published (40) crystallographic data. A simplified **NU-1000** pore model was constructed in Materials Studio software package. This pore model consists of four hexagonal rings of six Zr-oxide nodes each, extended along the *z* axis. We considered a number of functionalized structures with different arrangements of rotaxanes and dumbbells inside the hexagonal channel of **NU-1000**. See supporting information. The rotaxane moieties were attached to each Zr₆ node via two carboxylate oxygen atoms. In common with the orientations of perfluoroalkyl chains inside **NU-1000** that we have modeled previously (40), this functionalization of the framework results in the rotaxanes protruding along the vector of the hexagonal channel to some extent. All bonded and non-bonded interactions between framework atoms were described by the Universal Force Field and the structures were optimized using the Forcite module in Materials Studio.

ACKNOWLEDGEMENTS. We thank Dr Nicolaas A. Vermeulen for useful discussions and Xisen Hou for assistance in the preparation of Figure 2. This research is part (Project 34-949) of the Joint Center of Excellence in Integrated Nano-Systems (JCIN) at King Abdulaziz City for Science and Technology (KACST) and Northwestern University (NU). The authors would like to thank both KACST and NU for their continued support of this research. This material is based on work supported by the National Science Foundation (NSF) under CHE-1308107 (J.F.S) and CHE-1266201 (M.R.W.). P.R.M thanks the US–UK Fulbright Commission for an All-Disciplines Scholarship. I.H. thanks the US–Israel Fulbright Program for a Postdoctoral Fellowship. A.-J.A.

thanks the NSF for the award of a Graduate Research Fellowship (GRF) under the auspices of DGE-0824162. I.C.G.-H. is supported by a National Defense Science and Engineering Graduate (NDSEG) Fellowship from the Department of Defense under contract number FA9550-11-C-0028. N.E.H. was supported by the Department of Energy Office of Science Graduate Fellowship Program (DOE SCGF), made possible in part by the American Recovery and Reinvestment Act of 2009, administered by ORISE-ORAU under contract no. DE-AC05-06OR23100. A.K.B. acknowledges Fulbright New Zealand for a Fulbright Graduate Award and the New Zealand Federation of Graduate Women for a Postgraduate Fellowship Award. R.Q.S. acknowledges the Army Research Office (grant W911NF-12-1-0130) for financial support. Work in the lab of J.T.H. was supported by the U. S. Department of Energy, Office of Science, Office of Basic Energy Sciences, under grant No. DE-FG87ER13808, and by Northwestern University. O.K.F gratefully acknowledges funding from the Army Research Office (project number W911NF-13-1-0229).

References

1. Yaghi OM, et al. (2003) Reticular synthesis and the design of new materials. *Nature* 423:705–714.
2. Hupp JT, Poepplmeier KR (2005) Better living through nanopore chemistry. *Science* 309:2008–2009.
3. Férey G (2008) Hybrid porous solids: past, present, future. *Chem Soc Rev* 37:191–214.
4. Horike S, Shimomura S, Kitagawa S (2009) Soft porous crystals *Nature Chem* 1: 695–704.
5. Zhou H-C, Long JR, Yaghi OM (2012) Introduction to metal–organic frameworks. *Chem Rev* 112:673–674.
6. Getman RB, Bae Y-S, Wilmer CE, Snurr RQ (2012) Review and analysis of molecular simulations of methane, hydrogen, and acetylene storage in metal–organic frameworks. *Chem Rev* 112:703–723.
7. Farha OK, et al. (2010) De novo synthesis of a metal–organic framework material featuring ultrahigh surface area and gas storage capacities. *Nat Chem* 2:944–948.
8. Kreno LE, et al. (2012) Metal–organic framework materials as chemical sensors. *Chem Rev* 112:1105–1125.
9. Lee JY (2009) Metal–organic framework materials as catalysts. *Chem Soc Rev* 38:1450–1459.
10. Zhang T, Lin W (2014) Metal-organic frameworks for artificial photosynthesis and photocatalysis. *Chem Soc Rev* 43:5982–5993.
11. So, MC, Wiederrecht GP, Mondloch JE, Hupp JT, Farha OK (2015) Metal–organic framework materials for light-harvesting and energy transfer. *Chem. Commun.* 51:3501.
12. Deng H, Olson MA, Stoddart JF, Yaghi, OM (2010) Robust dynamics. *Nature Chem* 2:439–443.
13. Coskun A, Banaszak M, Astumian RD, Stoddart JF, Grzybowski BA (2012) Great expectations: can artificial molecular machines deliver on their promise? *Chem Soc Rev* 41:19–30.
14. Stoddart JF (2009) The chemistry of the mechanical bond. *Chem Soc Rev* 38:1802–1820.
15. Stoddart JF (2014) Putting mechanically interlocked molecules (MIMs) to work in tomorrow’s world. *Angew Chem Int Ed* 53:11102–11104.
16. Neal EA, Goldup SM (2014) Chemical consequences of mechanical bonding in catenanes and rotaxanes: isomerism, modification, catalysis and molecular machines for synthesis. *Chem Commun* 50:5128–5142.
17. Davidson GJE, Loeb SJ (2003) Channels and cavities lined with interlocked components: metal-based polyrotaxanes that utilize pyridinium axles and crown ether wheels as ligands. *Angew Chem Int Ed* 42:74–77.
18. Li Q, et al. (2010) A catenated strut in a catenated metal–organic framework. *Angew Chem Int Ed* 49:6751–6755.
19. Li Q, et al. (2010) A metal–organic framework replete with ordered donor–acceptor catenanes. *Chem Commun* 46:380–382.
20. Vukotic VN, Loeb SJ (2012) Coordination polymers containing rotaxane linkers. *Chem Soc Rev* 41:5896–5906.

21. Vukotic VN, Harris KJ, Zhu KL, Schurko RW, Loeb SJ (2012) Metal-organic frameworks with dynamic interlocked components. *Nature Chem* 4:456–460.
22. Coskun A, et al. (2012) Metal–organic frameworks incorporating copper-complexed rotaxanes. *Angew Chem Int Ed* 51:2160–2163.
23. Liang J, et al. (2013) Metal ion directed metal–organic rotaxane frameworks with intrinsic features of self-penetration and interpenetration. *Chem Commun* 49:8555–8557.
24. Cao D, et al. (2013) Three-dimensional architectures incorporating stereoregular donor–acceptor stacks *Chem Eur J* 19:8457–8465.
25. Vukotic VN, Loeb SJ (2014) Polyrotaxane metal-organic frameworks. *Metal-Organic Framework Materials*, eds MacGillivray LR, Luckehart CM (Wiley-VCH, Chichester), pp 115–134.
26. Zhu KL, Vukotic VN, O’Keefe CA, Schurko RW, Loeb SJ (2014) Metal-organic frameworks with mechanically interlocked pillars: controlling ring dynamics in the solid-state via a reversible phase change. *J Am Chem Soc* 136:7403–7409.
27. Collier CP, et al. (2000) A [2]catenane based solid-state electronically reconfigurable switch. *Science* 289:1172–1175.
28. Luo Y, et al. (2002) Two-dimensional molecular electronics circuits. *ChemPhysChem* 3:519–525.
29. Choi JW, et al. (2006) Ground state equilibrium thermodynamics and switching kinetics of bistable [2]rotaxane switches in solution, polymer gels, and molecular electronic devices. *Chem Eur J* 12:261–279.
30. Green JE, et al. (2007) A 160-kilobit molecular electronic memory patterned at 10^{11} bits per square centimeter. *Nature* 445:414–417.
31. Zhang W, et al. (2011) A solid-state switch containing an electronically switchable bistable poly[n]rotaxane. *J Mater Chem* 21:1487–4859.
32. Coskun A, et al. (2012) High hopes: can molecular electronics realize its potential? *Chem Soc Rev* 41:4827–4859.
33. Flood AH, Stoddart JF, Steuerman DW, Heath JR (2004) Whence molecular electronics? *Science* 306:2055–2056.
34. Li Q, et al. (2009) Docking in metal-organic frameworks. *Science* 325:855–859.
35. Garcia-Garibay MA (2005) Crystalline molecular machines: encoding supramolecular dynamics into molecular structure. *Proc Natl Acad Sci USA* 102:10771–10776.
36. Karlen SD, et al. (2010) Symmetry and dynamics of molecular rotors in amphidynamic molecular crystals. *Proc Natl Acad Sci USA* 107:14973–14977.
37. Sue AC-H, et al. (2015) Heterogeneity of functional groups in a metal-organic framework displays magic number ratios. *Proc Natl Acad Sci USA* 112:5591–5596.
38. Zhu K, O’Keefe CA, Vukotic VN, Schurko RW, Loeb SJ (2015) A molecular shuttle that operates inside a metal-organic framework. *Nature Chem* 7:xxx–xxx doi:10.1038/nchem.2258.
39. Clifford, T, Abushamleh A, Busch DH (2002) Factors affecting the threading of axle molecules through macrocycles: Binding constants for semirotaxane formation. *Proc Natl Acad Sci USA* 99:4830–4836.
40. Mondloch JE, et al. (2013) Vapor-phase metalation by atomic layer deposition in a metal–organic framework. *J Am Chem Soc* 135:10294–10297.
41. Mondloch JE, et al. (2014) Are Zr_6 -based MOFs water stable? Linker hydrolysis vs. capillary-force-driven channel collapse. *Chem Commun* 50:8944–8946.
42. Planas N, et al. (2014) Defining the proton topology of the Zr_6 -based metal–organic framework NU-1000. *J Phys Chem Lett* 5:3716–3723.
43. Deria P, et al. (2013) Perfluoroalkane functionalization of NU-1000 via solvent-assisted ligand incorporation: synthesis and CO_2 adsorption studies. *J Am Chem Soc* 135:16801–16804.
44. Deria P, Bury W, Hupp JT, Farha OK (2014) Versatile functionalization of the NU-1000 platform by solvent-assisted ligand incorporation. *Chem Commun* 50:1965–1968.
45. Deria P, et al., (2014) Beyond post-synthesis modification: evolution of metal–organic frameworks via building block replacement. *Chem Soc Rev* 43:5896–5912.
46. Deria P, et al. (2015) MOF functionalization via solvent-assisted ligand incorporation: phosphonates vs. carboxylates. *Inorg Chem* 54:2185–2192.

47. Monk PMS (1998) *The Viologens: Physicochemical Properties, Synthesis and Applications of the Salts of 4,4'-Bipyridine* (Wiley-VCH, New York).
48. Trabolsi A, et al. (2010) Radically enhanced molecular recognition. *Nature Chem* 2:42–49.
49. Li H, et al. (2010) Mechanical bond formation by radical templation. *Angew Chem Int Ed* 49:8260–8265.
50. Fahrenbach AC, et al. (2012) Solution-phase mechanistic study and solid-state structure of a tris(bipyridinium radical cation) inclusion complex. *J Am Chem Soc* 134:3061–3072.
51. Barnes JC, et al. (2013) A radically configurable six-state compound. *Science* 339:429–433.
52. Li H, et al. (2013) Mechanical bond-induced radical stabilization. *J Am Chem Soc* 135:456–467.
53. Barnes JC, (2014) et al. Solid-state characterization and photo-induced intramolecular electron transfer in a nanoconfined octacationic homo[2]catenane. *J Am Chem Soc* 136:10569–10572.
54. Witus LS, et al. (2014) Relative contractile motion of the rings in a switchable palindromic [3]rotaxane in water driven by radical-pairing interactions. *Org Biomol Chem* 12:6089–6093.
55. Cheng C, et al. (2014) Energetically demanding transport in a supramolecular assembly. *J Am Chem Soc* 136:14702–14705.
56. Bruns CJ, et al. (2014) Redox Switchable Daisy Chain Rotaxanes Driven by Radical-Radical Interactions. *J Am Chem Soc* 136:4714–4723.
57. Faust TB, D'Alessandro DM (2014) Radicals in metal-organic frameworks. *RSC Adv* 4:17498–17512.
58. Hod I, et al. (2014) Directed growth of electroactive metal-organic framework thin films using electrophoretic deposition. *Adv Mater* 26: 6295–6300.
59. Hod I, et al. (2015) Bias-switchable permselectivity and redox catalytic activity of a ferrocene-functionalized, thin-film metal-organic framework compound. *J Phys Chem Lett* 6:586–591.
60. Heath JR (2009) Molecular Electronics. *Annu Rev Mater Res* 39:1–23.
61. Allendorf MD, Schwartzberg A, Stavila V, Talin AA (2011) A roadmap to implementing metal-organic frameworks in electronic devices: challenges and critical directions. *Chem Eur J* 17:11372–11388.
62. Michl J, Sykes ECH (2009) Molecular Rotors and Motors: Recent Advances and Future Challenges. *ACS Nano* 3:1042–1048.
63. Vogelsberg CS, Garcia-Garibay MA (2012) Crystalline molecular machines: function, phase order, dimensionality, and composition. *Chem Soc Rev* 41:1892–1910.

Figure Legends

Figure 1. Leaders in the fields of MEDs, the internal dynamics of solids, and robust dynamics in MOFs. From left to right: Professors James (Jim) Heath, Omar Yaghi, Miguel Garcia-Garibay, and Stephen Loeb.

Figure 2. A timeline from 2000 to 2015 summarizing the progression of bistable MIMs from a single MSTJ fabricated using the LB technique to 160,000 MSTJs in a nanometer-sized device in 2007, followed by a summary to mount bistable MIMs inside MOFs. The present article describes our most recent contribution to this challenging area of research.

Figure 3. (A) Schematic of the Solvent-Assisted Ligand Incorporation (SALI) approach to organizing rotaxanes inside the channels of a metal-organic framework. A semirotaxane is formed under equilibrium conditions from a ring and a half-dumbbell component with a bulky stoppering group at one end. A functional group (red) at the other end of the linear component acts as an attachment point to anchor the semirotaxane within the **NU-1000** metal-organic framework. (B) An idealized representation of the structure of **NU-1000** based upon single-crystal X-ray diffraction (38).

Figure 4. (A) Structural formulas and graphical depictions of the semirotaxane components $\mathbf{1}^{2+}$ and \mathbf{CBPQT}^{4+} . (B) Formation of semirotaxane $\mathbf{1}^{\bullet+} \subset \mathbf{CBPQT}^{2(\bullet+)}$ occurs upon electrochemical reduction of $\mathbf{1}^{2+}$ and \mathbf{CBPQT}^{4+} with three moles of electrons, i.e., the one-electron reduction of each viologen subunit. (C) UV-Vis-NIR spectra (298 K, 2 mm path length) of an equimolar mixture of $\mathbf{1} \cdot 2\text{PF}_6$ and $\mathbf{CBPQT} \cdot 4\text{PF}_6$ (500 μM each) in a solution of Bu_4NPF_6 in deaerated MeCN (0.1 M) as a constant potential of -330 mV is applied. The blue trace corresponds to the spectrum before application of the potential and the purple trace shows the spectrum obtained after complete reduction. The near-infrared absorbance at 1167 nm is indicative of formation of the trisradical inclusion complex $\mathbf{1}^{\bullet+} \subset \mathbf{CBPQT}^{2(\bullet+)}$.

Figure 5. Spectroscopic characterization of **SALI-R**^{3(•+)}. (A) Partial ¹H NMR spectrum (500 MHz, 298 K) after digestion in a D₂SO₄–(CD₃)₂SO mixture. Integrals are shown for the resonances of protons corresponding to those labelled in Figs. 1B and 2A. (B) Solid-state UV-Vis-NIR reflectance spectra (powder, 298 K, 0.1 mm path length) of the three modified **NU-1000** frameworks prepared in this investigation. The broad peak centered around 1120 nm confirms the presence of $\mathbf{1}^{\bullet+} \subset \mathbf{CBPQT}^{2(\bullet+)}$ -derived rotaxanes in the channels of **SALI-R**^{3(•+)}.

Figure 6. Decay in the spectroscopic features associated with radical species upon exposing microcrystalline powder samples of **SALI-DB**^{•+} and **SALI-R**^{3(•+)} to air. In each case, the signals diminish rapidly on the hour timescale. (A) Comparison of the normalized EPR spectra of **SALI-DB**^{•+} and **SALI-R**^{3(•+)} under an inert N₂ atmosphere and (B) decay of the signal intensity with time upon exposure of the same samples to air. UV-Vis-NIR reflectance (powders, 298 K, path length 0.1 mm) at 648 nm and 1120 nm (i.e., the mono- and -trisradical bands, respectively) increases in intensity after exposure to air of (C) **SALI-DB**^{•+} and (D) **SALI-R**^{3(•+)}.

Figure 7. Molecular mechanics models of a short section of the hexagonal pore of **NU-1000** containing dumbbells and rotaxanes distributed in a manner that is representative of **(A)** a 1:1 ratio of exogenous carboxylates to Zr clusters (three within each hexagonal section) and **(B)** a 2:1 ratio (six dumbbells or rotaxanes within a single hexagonal section). A 1:1 ratio of dumbbells to rotaxanes (three of each) was chosen to match the experimentally measured distribution of components in **SALI-R^{3(•+)}**. The computed relative energies are given below, alongside simplified graphical representations of the models.

Figure 8. Solid-state electrochemistry. **(A)** A thin film of **SALI-R^{3(•+)}** crystals on a FTO electrode. **(B)** Cyclic voltammetry acquired at a scan rate of 50 mVs⁻¹ reveals a semi-reversible redox wave centered around -250 mV, corresponding to the one-electron reduction of the viologen components of **SALI-R^{3(•+)}**. **(C)** The change in current density over time after a step in applied potential from 100 V to -700 mV.



Figure 1

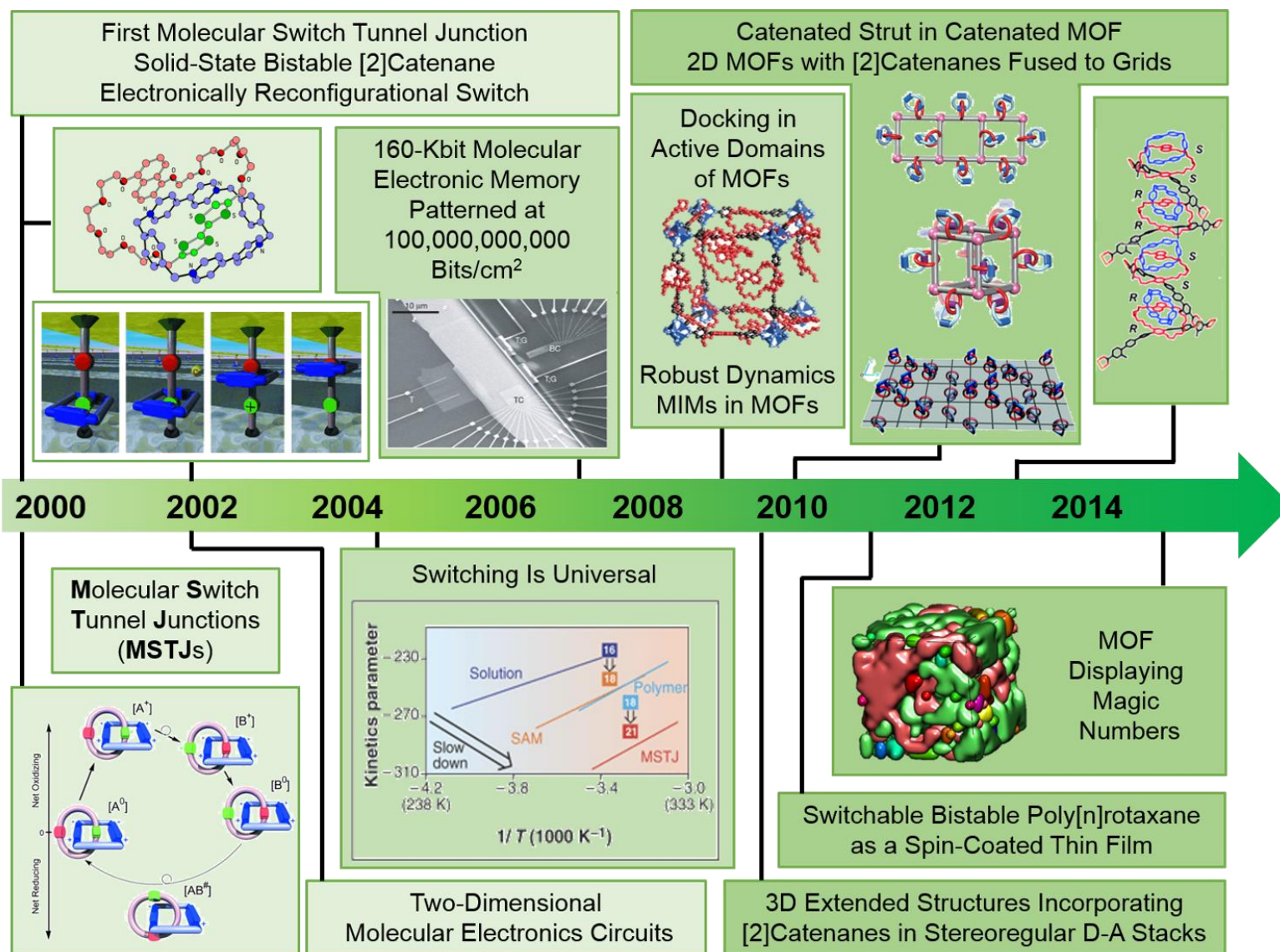


Figure 2

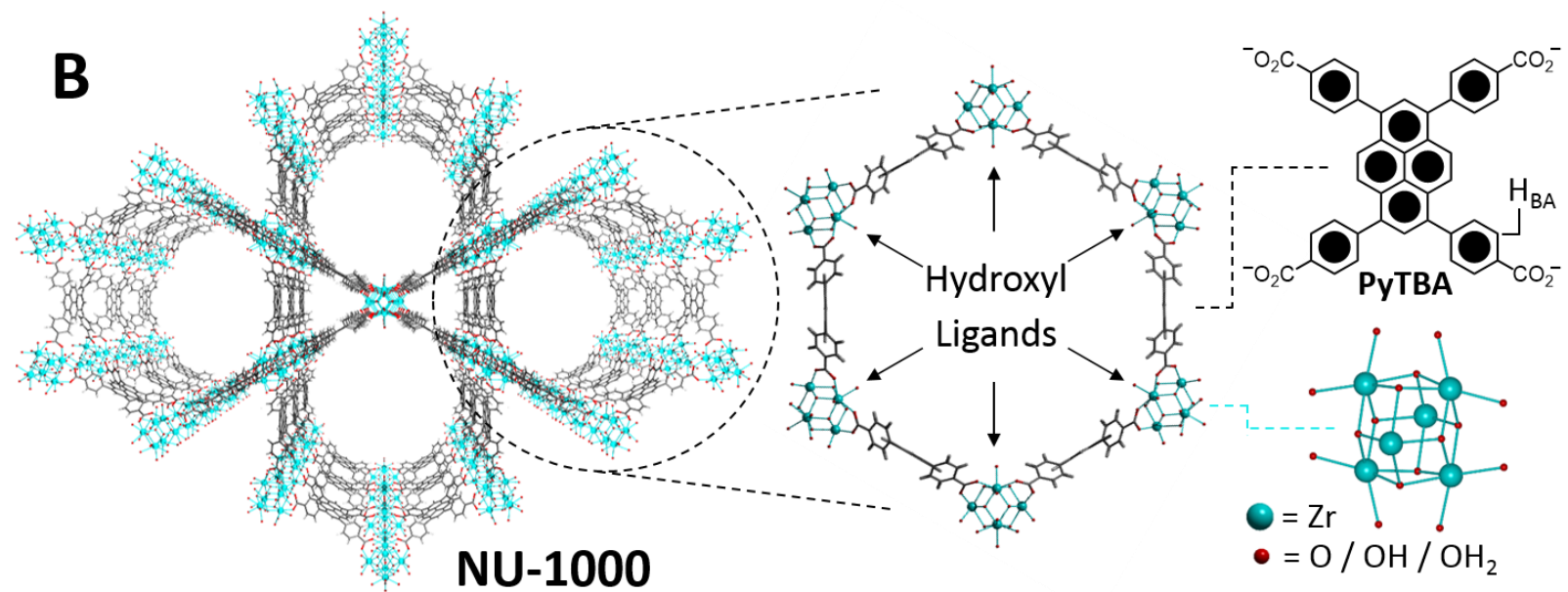
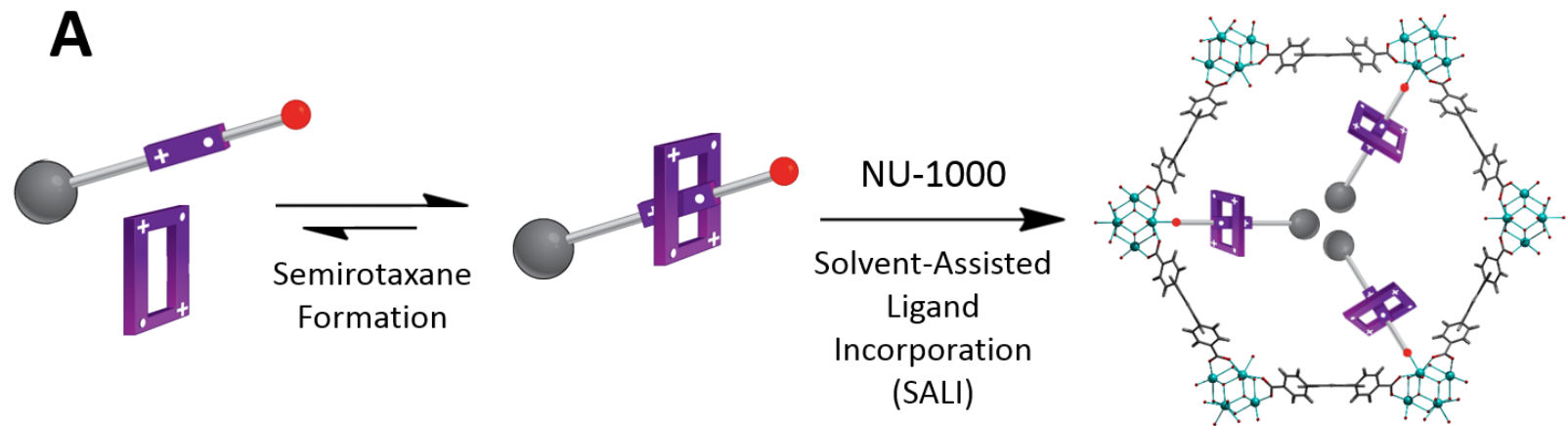


Figure 3

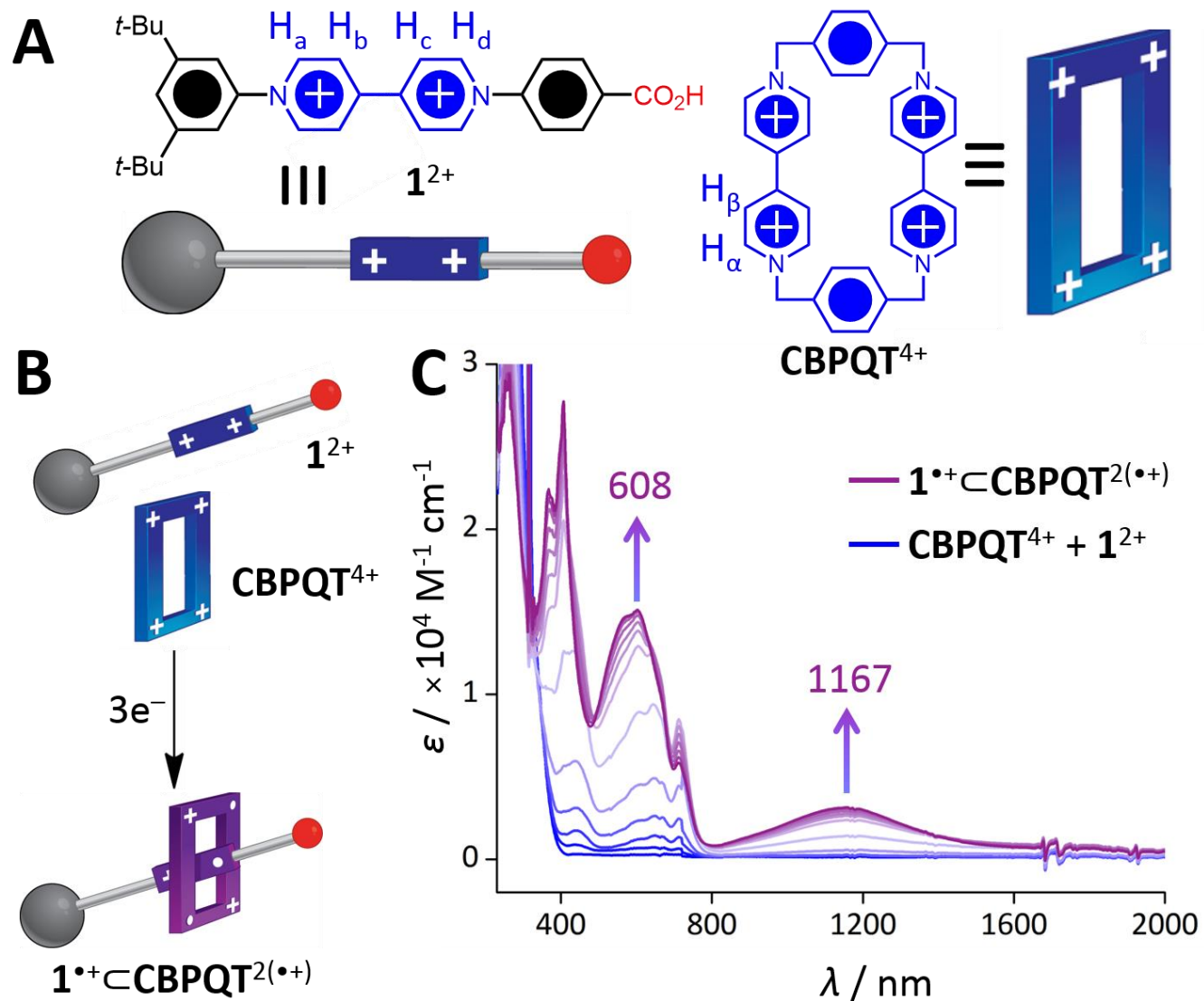


Figure 4

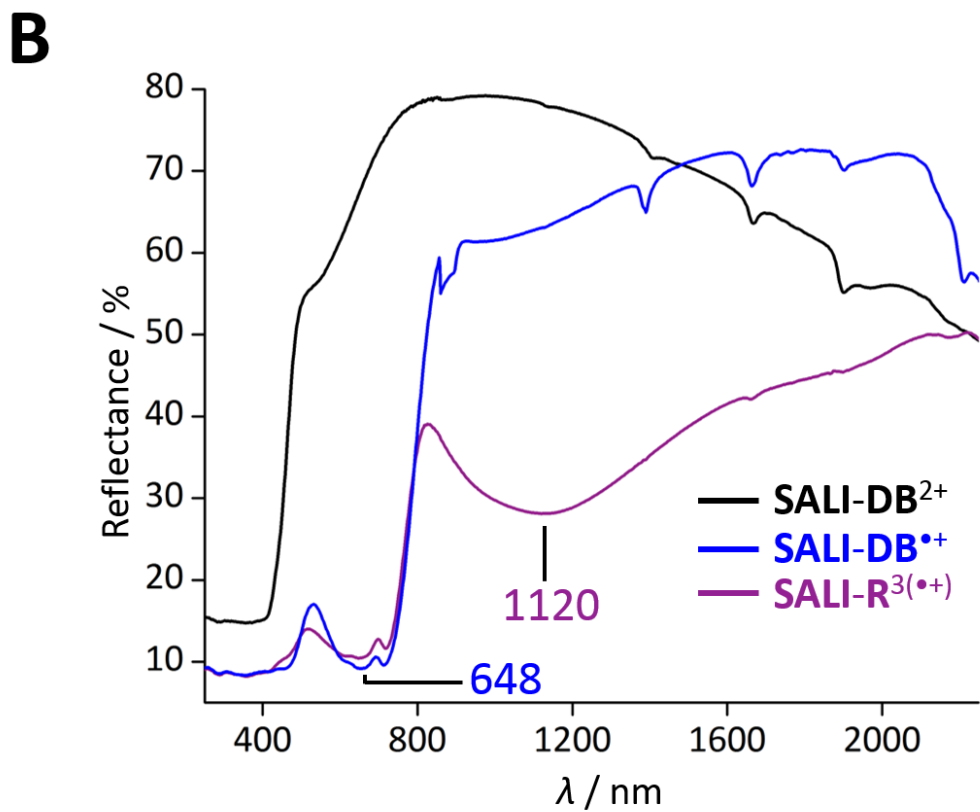
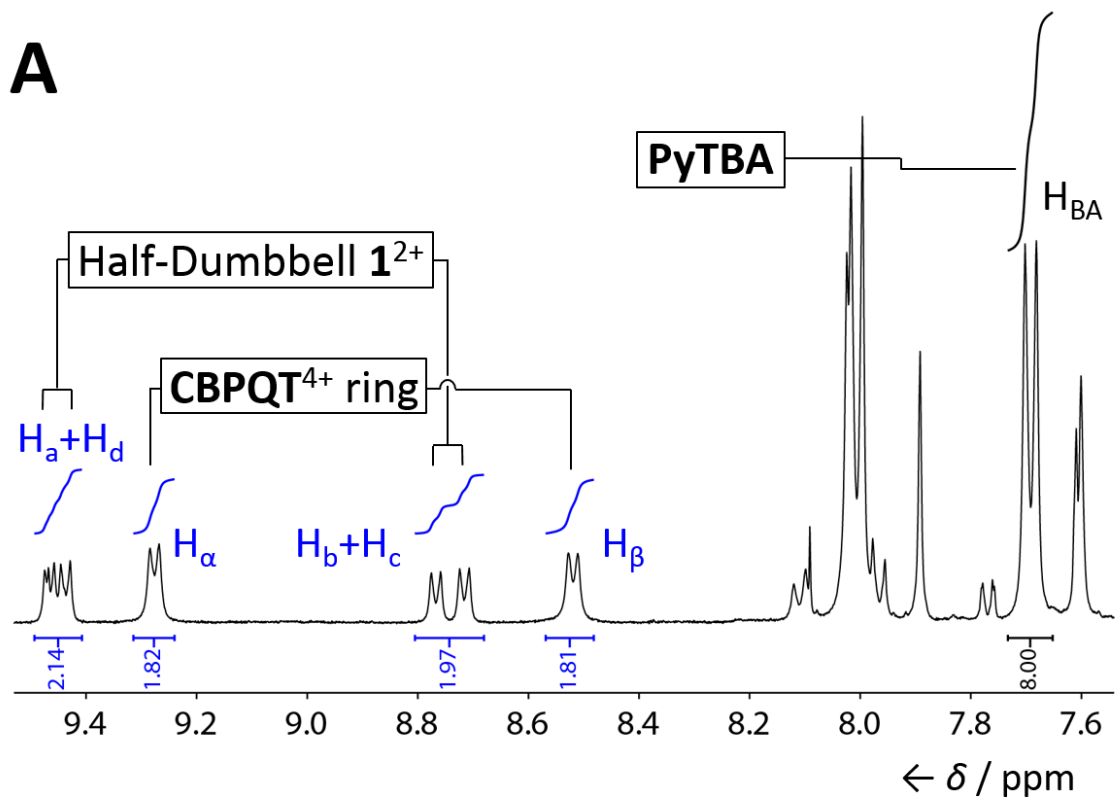


Figure 5

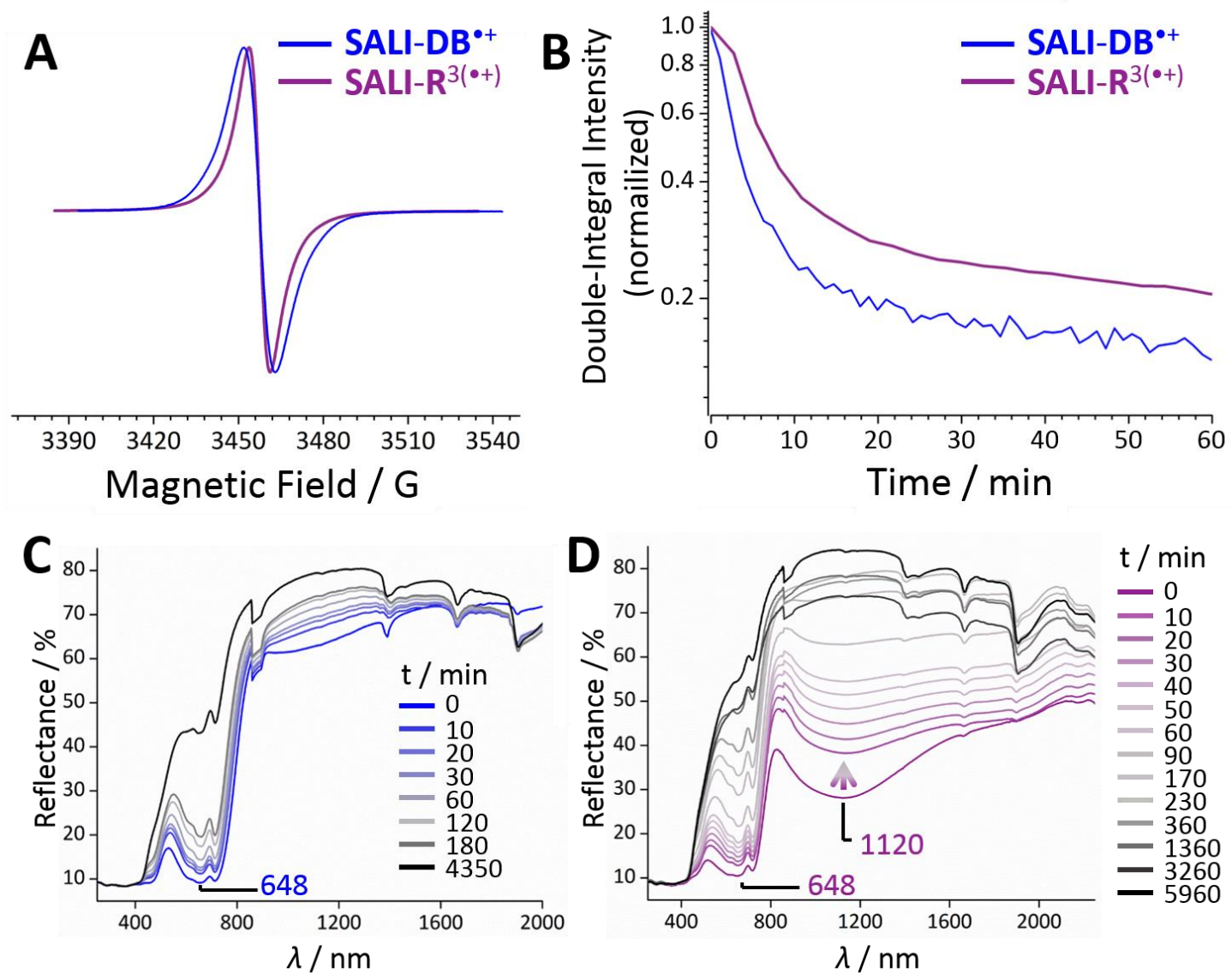


Figure 6

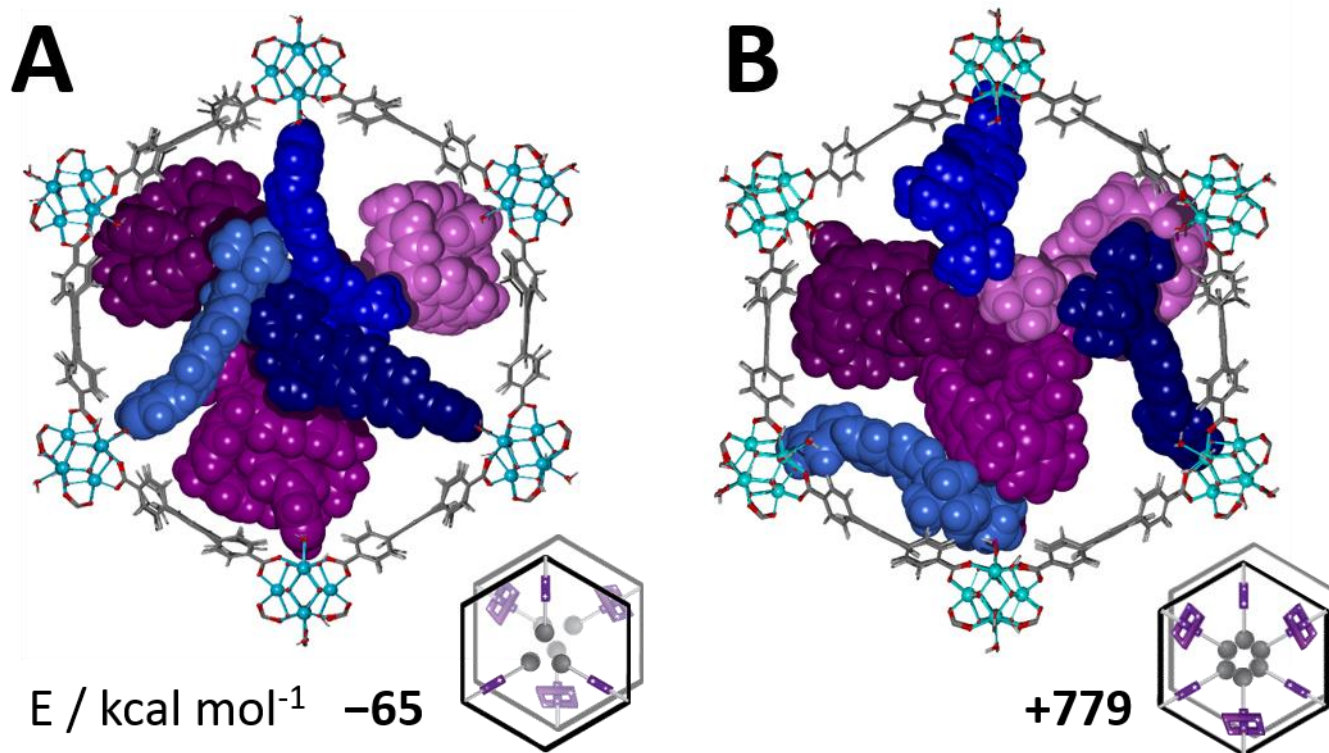


Figure 7

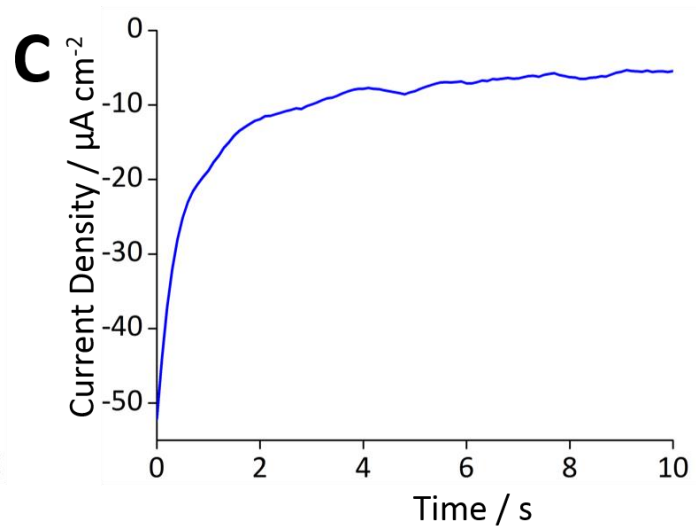
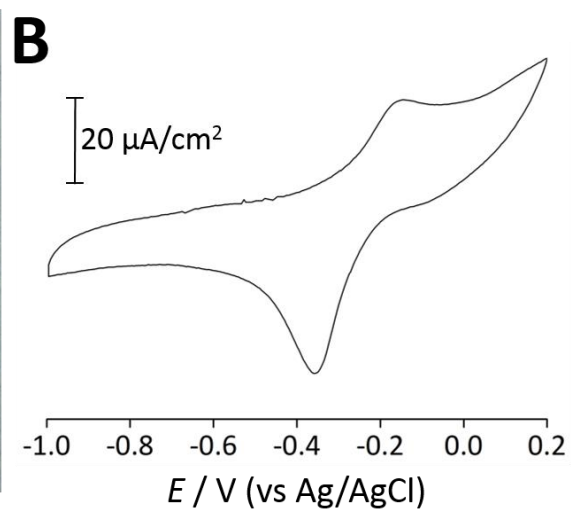
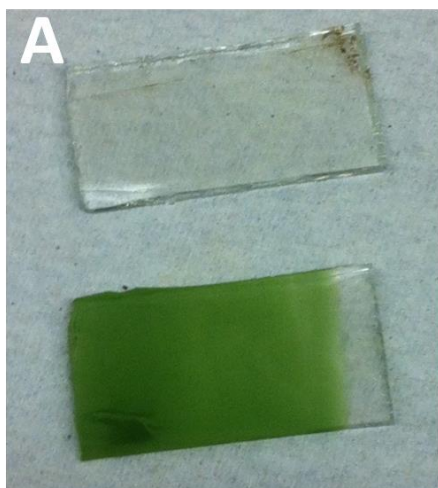


Figure 8